Journal of
Materials Chemistry C

Materials for optical, magnetic and electronic devices

Accepted Manuscript

This article can be cited before page numbers have been issued, to do this please use: C. Huang, S. Ho, C. Lai, C. Ko, Y. Wei, J. Lin, D. Chen, T. Ko, K. Wong, Z. Zhang, W. Hung and P. Chou, *J. Mater. Chem. C*, 2020, DOI: 10.1039/D0TC00986E.

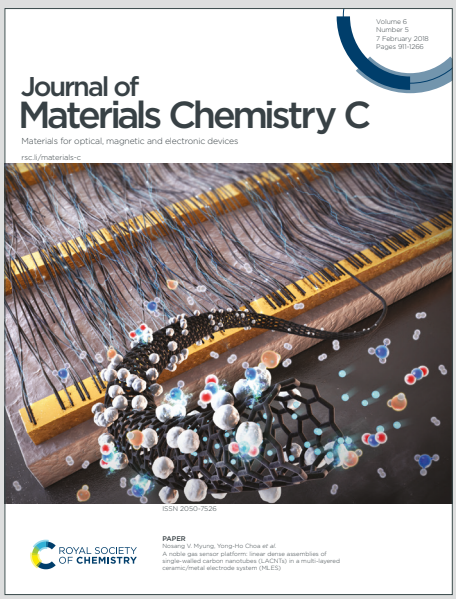

ROYAL SOCIETY OF CHEMISTRY

rsc.li/materials-c

View Article Online
DOI: 10.1039/D0TC00986E

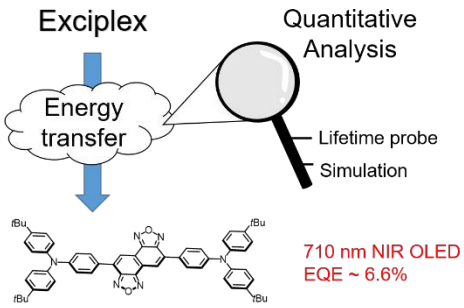

Insight into the energy transfer pathways between the exciplex host and NIR fluorescence chromophores.

View Article Online
DOI: 10.1039/D0TC00986E

ARTICLE

Insights into Energy Transfer Pathways between Exciplex Host and Fluorescent Guest: Attaining Highly Efficient 710 nm Electroluminescence.

Received 00th January 20xx,
Accepted 00th January 20xx

DOI: 10.1039/x0xx00000x

Chun-Ying Huang,[1,‡] Ssu-Yu Ho,[1,‡] Chien-Hsun Lai,[2] Chang-Lun Ko,[2] Yu-Chen Wei,[1] Jia-An Lin,[1] Deng-Gao Chen,[1] Tzu-Yu Ko,[1] Ken-Tsung Wong,[1] Zhiyun Zhang,[3,*] Wen-Yi Hung,[2,4,*] and Pi-Tai Chou[1,*]

Energy transfer between exciplex host and fluorescent guest becomes one of the demanding processes to attain high performance of the organic light emitting diodes (OLEDs), especially in the near infrared (NIR) region. However, the insight into the dynamics of energy transfer remains elusive. In this study, new deep red/NIR chromophores **NOz-TPA** and **NOz-t-TPA** where NOz and TPA denote naphthobisoxadiazole and triphenylamine, respectively, are developed with an electron donor-acceptor-donor (D-A-D) configuration. The optimized 1 wt% doped films for **NOz-TPA** and **NOz-t-TPA** blended with Tris-PCz:CN-T2T (1:1 in molar ratio) exciplex host show similar deep red/NIR emission with photoluminescence quantum yields (PLQY) of 42 (680 nm) and 28%, (709 nm), respectively. Comprehensive time resolved measurements and dynamics analyses reveal significant differences in energy transfer pathways, i.e. Förster versus Dexter type energy transfer, between exciplex host and the fluorescent guest, in which the introduction of bulky *tert*-butyl groups in the **NOz-t-TPA** doped film greatly suppresses Dexter type energy transfer pathway. Despite lower PLQY, the analytical simulation predicts **NOz-t-TPA** to be a better candidate to realize a highly efficient electroluminescence. The confirmation is then given by the performance of **NOz-t-TPA** doped OLED, showing an external quantum efficiency (EQE) of 6.6% with peak wavelength at 710 nm, which is among the best records for the metal-free NIR OLEDs around 710 nm. The insight of energy transfer pathways thus plays a pivotal role to achieve the high performance OLEDs that incorporate exciplex host and fluorescent guest.

Introduction

Since the first demonstration by Tang and VanSlyke in 1987, organic light-emitting diodes (OLEDs) have attracted worldwide attention.[1] With decades of effort, researches and developments of OLEDs have gained significant improvement in the field of display panels and light sources.[2-4] Recently, it becomes recognized that energy transfer between exciplex host and regular fluorescent guest provides a facile means to promote OLED performance.[5-7] In this approach, the thermally activated delay fluorescence (TADF) exciplex material serves as a host to harvest both the singlet and triplet population, followed by Fŏrster type energy transfer (FRET) to the fluorescent guest. As such, the upper-limit on external quantum efficiency (EQE) of conventionally fluorescent device can be overcome. This strategy provides three manifolds in benefit. First, the pure metal-free fluorescent devices have the advantage of lower cost compared to that of the heavy-metal based devices. Second, the small concentration used for the fluorescent dopants may minimize the serious decrease in EQE under high current density, i.e. a roll off process, while this phenomenon is commonly observed among phosphorescence devices due to triplet-triplet and/or triplet-polaron annihilation.[8] Third, the fine tuning of spectral range of device can be easily accessed by varying the suitable combination of exciplex host and fluorescence dopants. In this aspect, the use of exciplex for the energy transfer materials also features its facility for synthesis and versatility in wide tuning the emission region compared with those of intramolecular TADF molecules.The promotion of OLEDs' performance at different spectrum window can thus be achieved with straightforward design.[6] Nevertheless, it should be addressed that Dexter type energy transfer (DET), which transfers the energy from the triplet state of host TADF material to the triplet state of fluorescent guest, should be avoided as much as possible.[9] In this aspect, it is surprising that the detailed discussion on energy transfer remains elusive.

In yet another approach, near-infrared (NIR) OLEDs show great perspective in optical communication,[10] phototherapy,[11] night-vision technologies,[12] and sensors.[13-15] Many research teams have pursued boosting the performance of deep-red/NIR OLEDs,[16-25] of which the efficiency is generally low as the deep-red/NIR emission intensities are limited by the energy gap

[a.] *Department of Chemistry, National Taiwan University, Taipei, 10617, Taiwan, R.O.C.*
[b.] *Department of Optoelectronics and Materials Technology, National Taiwan Ocean University, Keelung 202, Taiwan, R.O.C.*
[c.] *Key Laboratory for Advanced Materials and Institute of Fine Chemicals, East China University of Science & Technology, Shanghai 200237, P.R. China.*
[d.] *Center of Excellence for Ocean Engineering, National Taiwan Ocean University, Keelung, 202, Taiwan, R.O.C.*

† Electronic Supplementary Information (ESI) available. See DOI: 10.1039/x0xx00000x

‡ These authors contribute equally.

View Article Online
DOI: 10.1039/D0TC00986E

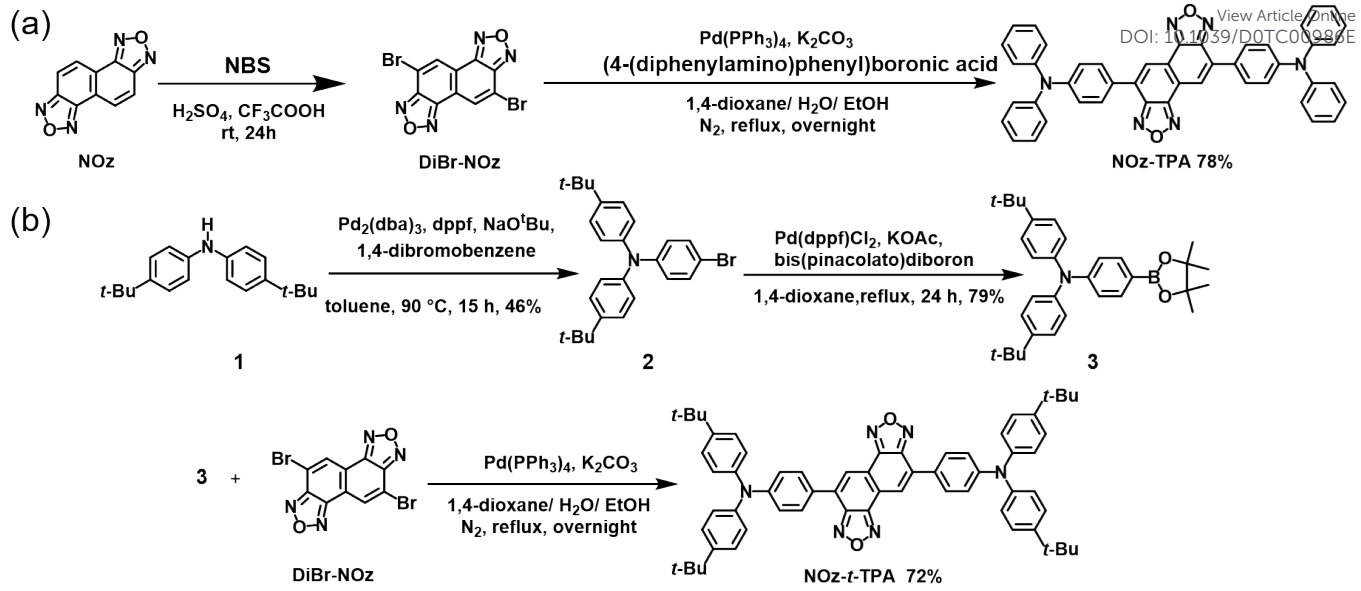

Scheme 1 Synthetic pathways for (a) **NOz-TPA** and (b) **NOz-t-TPA**.

law.[26-27] The heavy-metal based devices such as Pt-based porphyrin complexes generally showed remarkable EQE within NIR region,[28] but serious roll-off (*vide supra*). On the other hand, a number of organic molecules possessing thermally activated delay fluorescence (TADF) in the red and NIR region were reported to have highly efficient NIR OLEDs.[17-18, 29-31] However, the design and synthesis of NIR emitters having TADF properties is nontrivial and a great challenge, which may hamper their further advance. The quest of highly efficient NIR OLEDs with straightforward design is thus in urgency. In this regard, the aforementioned energy-transfer strategy from exciplex host to NIR fluorescent dopants provides an alternative opportunity. In this approach, design of deep red/NIR organic dyes may be accessed via extending planar π-conjugation, so that the delocalization of π-electron can narrow the energy gap, while the rigid planar structures can suppress the rotational disorder and hence decrease the non-radiative relaxation process.[32] Combined with exciplex material possessing green-yellow emission, the NIR emission can be reached by a variety of organic fluorescence materials endowed with electron donor-acceptor-donor (D-A-D) architectures through FRET.[17, 33-36]

Herein, we present two new deep red/NIR chromophores **NOz-TPA** and **NOz-t-TPA** (Scheme 1) where NOz and TPA denote naphthobisoxadiazole and triphenylamine, respectively, configured with an electron donor-acceptor-donor (D-A-D) structure. NOz belongs to the category of naphthobischalcogenadiazole (NXz). NXz is a tetracyclic heteroaromatic ring and has been utilized in the field of solar cell as the acceptor unit in semiconducting polymer,[37-40] affording low lying lowest unoccupied molecular orbital (LUMO) and rigid planar structure. In 2014, Michiaki et al. synthesized naphthobisthiadiazole (NTz)-based highly emissive red dyes.[41] Comparing NTz, naphthobisoxadiazole (NOz), in which the sulfur atom of NTz is substituted by oxygen, is expected to reach even lower LUMO than that of NTz due to the stronger withdrawing-ability of oxygen, narrowing the energy gap to the NIR region.[37] None of the D-A-D emitters based on NOz as the acceptor, so far, have been developed.

In this study we not only strived to attain high performance NIR OLEDs based on the energy transfer methodology between exciplex host and **NOz-TPA** (or **NOz-t-TPA**) fluorescent guest; more importantly, we made comprehensive time resolved measurements and dynamics analyses in an aim to gain insights into the energy transfer pathways. Despite the structure similarity between **NOz-TPA** and **NOz-t-TPA** they surprisingly reveal significant difference in energy transfer pathways, i.e. Förster versus Dexter type energy transfer. Albeit lower photoluminescence quantum yield (PLQY) for **NOz-t-TPA** doped in a host matrix, analytical simulation based on relaxation dynamics predicts its better electroluminescence yield due to the much suppressed DET. Affirmation is then given by the high performance of **NOz-t-TPA** doped OLED, showing an external quantum efficiency (EQE) of 6.6% with peak wavelength at 710 nm. The agreement between analytical approach and the performance of fabricated OLEDs sheds light on the mechanism to ascertain high performance NIR OLEDs via energy transfer. Detail of results and discussion is elaborated below.

Results and Discussion

Synthesis and characterization

The synthetic pathways for **NOz-TPA** and **NOz-t-TPA** are depicted in Scheme 1. In brief, 5,10-dibromonaphtho[1,2-c:5,6-c]bis([1,2,5]oxadiazole (DiBr-NOz) was synthesized following the procedure described in the literature,[37] which was then used to prepare the designated compound **NOz-TPA** via Suzuki coupling and Buchwald-Hartwig reaction. Compound **3**, which is one of the starting materials of **NOz-t-TPA**, was synthesized from the commercially available reagent bis(4-tert-butylphenyl)amine (1). **1** was then reacted with 1,4-dibromobenzene to yield **2** through Buchwald-Hartwig reaction.

View Article Online
DOI: 10.1039/D0TC00986E

Table 1. Photophysical properties of **NOz-TPA** and **NOz-t-TPA**

compound	λ_{max}^{abs} (nm)[a]		λ_{max}^{em} (nm)[b]		Φ (%)		τ (ns)		k_r ($10^7 s^{-1}$)[c]	
	TOL	neat film	TOL	neat film	TOL	neat film	TOL	neat film	TOL	neat film
NOz-TPA	548	570	653	730	40	22	4.54	0.43(30%) 3.44(70%)	8.81	8.67
NOz-t-TPA	570	586	675	750	35	6.8	4.59	0.16(71%) 0.82(29%)	7.62	19.3

Notes that TOL represents toluene. [a]The wavelength was recorded from the maximum value of the first band. [b]The wavelength was recorded from the maximum value of the emission spectra. [c]Radiative decay rate constant (k_r) was calculated according to the equation $k_r=\Phi/\tau$.

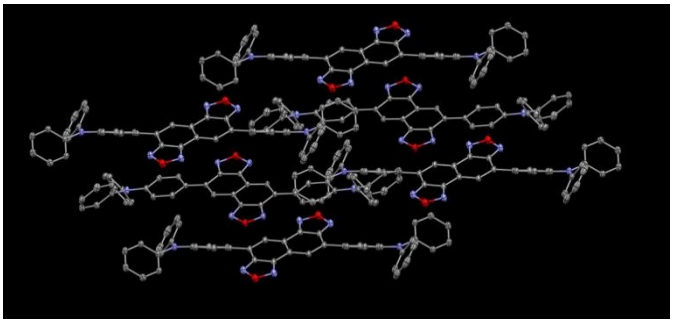

Figure 1. Packing structure of **NOz-TPA** in its single crystal. The thermal ellipsoid is shown at the 30% probability level with hydrogen atoms omitted for clarity.

Borylation of **2** with bis(pinacolato)diboron gave **3** which was used to prepare the designated compound **NOz-t-TPA** via Suzuki coupling by reacting with DiBr-NOz that has been elaborated in previous steps (*vide supra*). Details of synthetic routes are provided in Electronic Supplementary Information (**ESI**).

All synthesized compounds were characterized by ^1H and ^{13}C NMR spectroscopy. The corresponding crystal and packing structures obtained from X-ray structural analysis are shown in Figure 1. The packing mode of **NOz-TPA** exhibits relatively close intermolecular distance, which are around 3.4Å measured from the centroid of acceptor to the plane made by the neighboring acceptor. This relatively close intermolecular distance may lead to slight intermolecular interaction and result in spectral shift from solution to the solid phase (*vide infra*). Attempts to grow single crystal of **NOz-t-TPA** unfortunately were not successful, due perhaps to the involvement of bulky donor moiety. Nevertheless, it may be safely to expect that **NOz-t-TPA** has similar but less ordered architecture than that of **NOz-TPA** because of bulky t-TPA group. Thermogravimetric analysis (TGA) was recorded on a TA Q500 under nitrogen atmosphere at a heating rate of 5 °C/min. The temperature of 5% weight loss (Td) was at 362 °C for both **NOz-TPA** and **NOz-t-TPA**. The high thermal decomposition temperatures reveal their good thermal stability.

Photophysical properties

The UV/Vis absorption and emission spectra of title compounds in various solvents are recorded in Figure 2(a), and Table 1 (detailed data are listed in Table S1). The lowest lying absorption band of **NOz-TPA** and **NOz-t-TPA** with absorption peak at 548 and 570 nm, respectively, are ascribed to the ππ* transition mixed with donor-to-acceptor charge transfer (CT) character. This statement is supportive by their high extinction coefficients (ε) of > 10^4 $M^{-1}cm^{-1}$ at peak wavelength and the computational approach based on the time-dependent density functional theory (TD-DFT, cam-B3LYP hybrid function, see **ESI** for computational details).[42] As shown in Table S2, the highest occupied molecular orbital (HOMO) and LUMO for title compounds are all mainly located on the donors (TPA, t-TPA) and acceptor (NOz), respectively, manifesting an intramolecular charge transfer (ICT) from donors (t-TPA, TPA) to acceptor (NOz). In addition to the ICT event, the central acceptor shows part of ππ* transition character with obvious overlap between

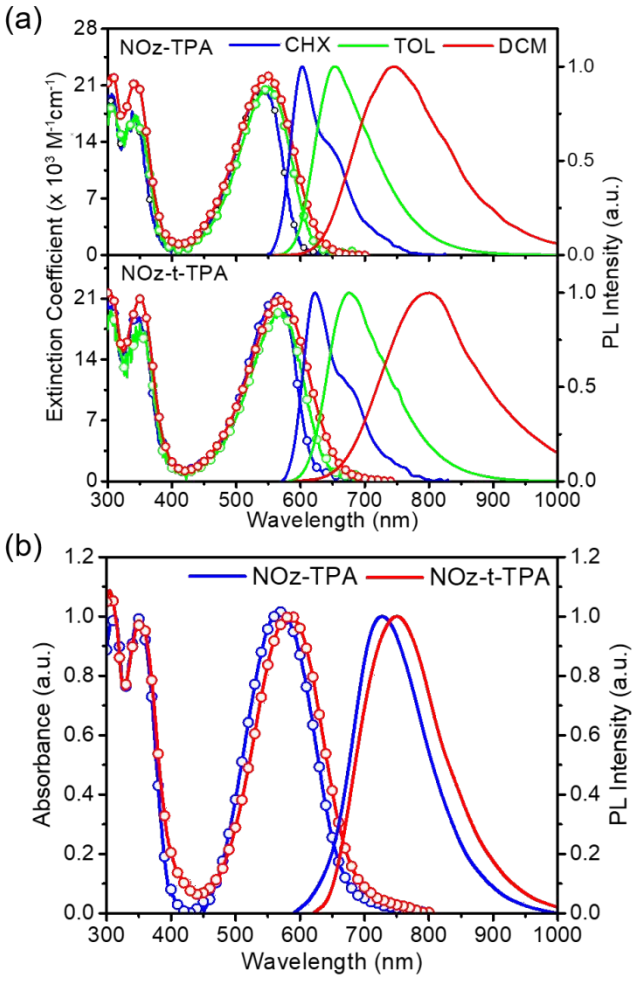

Figure 2. (a) Absorption spectra (lines with circles) and emission spectra of **NOz-TPA** and **NOz-t-TPA** in various solvent. Note that CHX, TOL, DCM denote cyclohexane, toluene, and dichloromethane, respectively. (b) Normalized absorption and emission spectra of **NOz-TPA** and **NOz-t-TPA** in neat film.

HOMO and LUMO on the six-membered aromatic rings.

View Article Online
DOI: 10.1039/D0TC00845

Therefore, the introduction of such acceptors provides strong electron-withdrawing character and thus the elongation of the π-electron delocalization, enhancing optical transition probability. In terms of **NOz-t-TPA**, replacement of TPA with t-TPA further enhances the electron-donating strength compared to **NOz-TPA**, leading to the lift of HOMO energy and hence the decrease of the absorption energy gap. The emission spectra of title compounds are red shifted as increasing the polarity of solvents, showing positive solvatochromism. For example, in dichloromethane (DCM), the emission peak wavelength of both title compounds shifts to NIR region, with the emission peak wavelength of **NOz-t-TPA** (800 nm) > **NOz-TPA** (746 nm). Remarkably, QY of both **NOz-TPA** and **NOz-t-TPA** were measured to be 40% and 35%, respectively, for 653 nm and 675 nm emission in toluene.

In the solid neat film, shown in Figure 2(b), both absorption and emission bands of **NOz-TPA** and **NOz-t-TPA** are red shifted compared with those observed in toluene. Due to the lack of fast environment relaxation in solid, such a red shift manifests the influence of static intermolecular interaction, in part, in solid state. Importantly, the emission bands for **NOz-TPA** and **NOz-t-TPA** in solid neat film have reached the NIR range with peak wavelength at 730 and 750 nm, and retaining good QY of 22% and 6.8%, respectively. We then measured the population lifetime of title compounds in the selected solvents and neat films (Figure S1-2) with pertinent data listed in Table 1 and Table S1. In all cases, the population lifetime of title compounds can be fitted well with exponential decay in the nanosecond range, implying their fluorescence nature. These, together with the measured data of QY, lead us to deduce the corresponding radiative rates (k_r), which all exhibit a fast radiative rate around ~10^8 s^{-1} (Table 1), clearly suggesting an efficient optical transition between lowest singlet excited state (S_1) and ground state (S_0).

In light of the high transition moment and excellent fluorescence yield in NIR for title compounds, we have investigated their PL performance under host-guest system. In this aspect, exciplex is chosen as the cohost in an aim to realize their high efficiency OLEDs via energy transfer.[43] Exciplex is formed with charge-transfer characters between electron-donating and electron-accepting molecules, which shows intrinsically small ΔE_{ST} due to the suppression of electron correlation energy and allows the triplet excitons up-converting to their singlet state by reverse intersystem crossing (RISC) process. Hence, the singlet excitons of exciplex cohost can transfer directly to singlet state of the fluorescent dopants via FRET pathway.[5] Additionally, to suppress the possibility of undesired Dexter process that depletes the triplet state, the

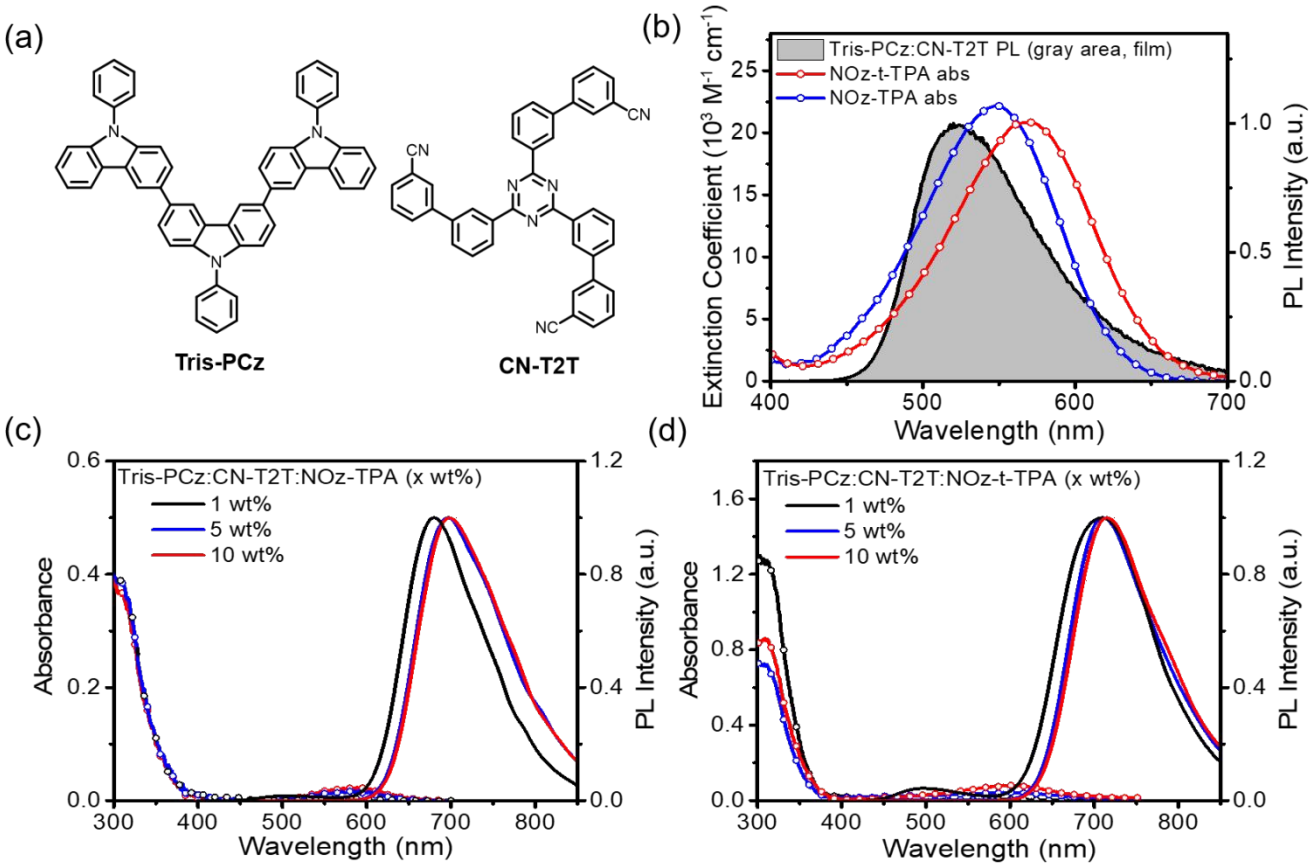

Figure 3. (a) Chemical structures of Tris-PCz and CN-T2T. (b) Overlap of photoluminescence (PL) spectrum (gray area) of the exciplex Tris-PCz:CN-T2T (1:1) and absorption spectrum (line with dots) of the dopants **NOz-TPA** and **NOz-t-TPA** in dichloromethane. (c,d) Absorption (line with dots, left side) and emission spectra (right side) of Tris-PCz:CN-T2T:(c) **NOz-TPA** and (d) **NOz-t-TPA** in various doping concentration. λ_{ex} = 310 nm for (c,d).

View Article Online
DOI: 10.1039/D0TC00986E

Table 2. Photophysical properties of Tris-PCz:CN-T2T:dopant (x wt%) blend film.

Dopant	x wt%[a]	λ_{peak} (nm)[b]	QY (%)	τ_{obs}/ns (pre-exponential factor)
NOz-TPA	1	680	42	0.692 (-0.391), 10.8 (0.605), 131 (0.003)
	5	697	29	4.54 (0.552) 8.61 (0.446), 43.1 (0.003)
	10	698	29	3.30 (0.450), 7.82 (0.545), 31.5 (0.004)
NOz-t-TPA	1	709	28	0.893 (-0.412), 9.30 (0.584), 252 (0.004)
	5	710	26	4.43 (0.418), 10.4 (0.019), 99.1 (0.000)
	10	715	20	3.34 (0.967), 9.43 (0.033)

[a] Doping concentration represented by percentage in weight. [b]Peak wavelength of emission band from dopants.

concentration of dopants needs in a suitably low level to keep an effective long-range singlet-singlet energy transfer in the system.

Here, we selected the highly efficient delayed fluorescent exciplex of 9,9′,9″-triphenyl-9H,9′H,9″H-3,3′:6′,3″-tercarbazole (Tris-PCz)[44]: 3′,3‴,3⁗,3⁗′-(1,3,5-triazine-2,4,6-triyl)tris(([1,1′-biphenyl]-3-carbonitrile)) (CN-T2T)[45] by 1:1 weight ratio as cohost (Figure 3(a)). The Tris-PCz:CN-T2T (1:1) exciplex emission shows a high Φ_{PL} of 0.53 and a small ΔE_{ST} = 0.59 kcal/mole, which leads to a highly efficient green exciplex OLED with EQE of 11.9%.[6] To realize an effective FRET, spectrum overlap between the emission of the host (energy donor) and the absorption of the dopant (energy acceptor) is required.[46] Figure 3(b) displays the region of overlap between the absorption spectra of dopants and the PL spectrum of Tris-PCz:CN-T2T, which allows efficient energy transfer from the exciplex to the dopants. Figure 3(c) shows the absorption and emission spectra of the doped films in various doping concentration represented by percentage in weight (wt%) versus the host. For the doping concentration of 1 wt%, the first absorption band (locating around 550 ~ 600 nm) as well as the highly energetic absorption band (300~400 nm) of dopants (**NOz-TPA** and **NOz-t-TPA**) couldn't be measured (absorbance < 0.005). Therefore, the corresponding emission spectra shown in Figure 3(c,d) excited at 310 nm unambiguously result from the energy transfer from the exciplex host. Comparing that of the **NOz-TPA** 1 wt% doped film (Figure 3c), the **NOz-t-TPA** 1 wt% doped film has obvious residue emission from exciplex at ~500 nm (Figure 3d), suggesting its less efficiency in energy transfer. This observation can be rationalized, in a qualitative manner, by the less spectrum overlap between PL spectrum of exciplex and absorption spectrum of **NOz-t-TPA** (Figure 3(b)). The photophysical properties of doped films are collected in Table 2. PLQY of 1 wt% doped films (Tris-PCz:CN-T2T:dopant (1 wt%)) were measured to be 42 and 28% for **NOz-TPA** (680 nm emission) and **NOz-t-TPA** (709 nm emission), respectively.

To acquire the preliminary information of parameters that corresponds to the energy transfer inside the doping system, we conducted the lifetime measurements with time correlated single photon counting (TCSPC) system incorporating a 0.82MHz femtosecond laser (180 fs pulse duration) and multichannel plate as pump pulse and detecting system, respectively, so that a temporal resolution of as short as 20 ps

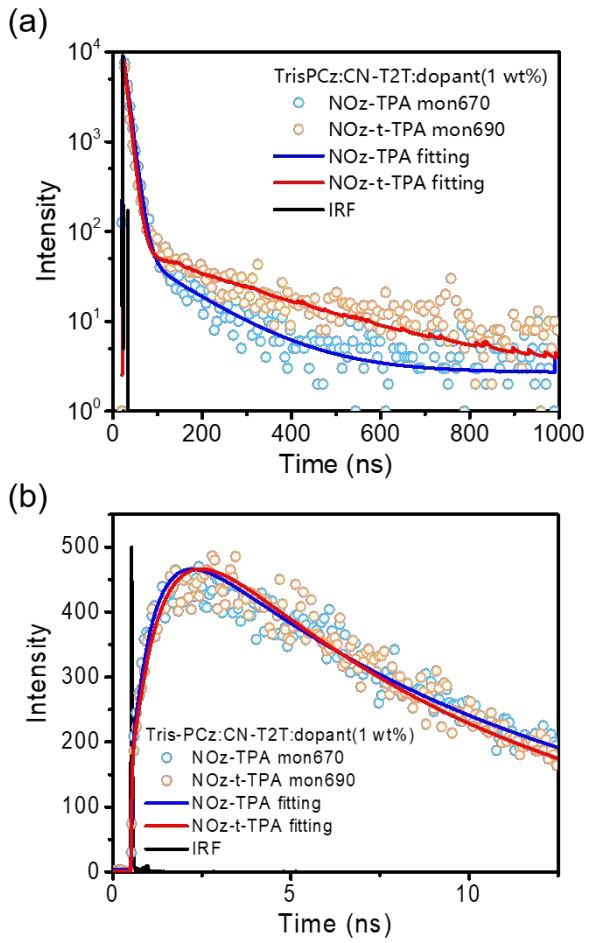

Figure 4. Observed population decay of Tris-PCz:CN-T2T:1 wt% **NOz-TPA** / **NOz-t-TPA** doped film monitored at 670 / 690 nm with excitation at 357 nm. (a) TADF character of the emission from the corresponding doped film. (b) Rise trajectory of the emission from the corresponding doped film.

can be obtained. The population decay of the emission of **NOz-t-TPA** and **NOz-TPA** 1 wt% doped film (Figure 4(a), Table 2), of which the corresponding decay curves can be well fitted by two single exponential components, which are 9.30 and 252 ns for **NOz-t-TPA** (monitored at 690 nm), 10.8 and 131 ns for **NOz-TPA** (monitored at 670 nm), respectively, denoted as prompt and delayed fluorescence decay. These results suggest the TADF characters for both emissions from **NOz-TPA** and **NOz-t-TPA**

View Article Online
DOI: 10.1039/D0TC00965E

due to the energy transfer from TADF of exciplex in the doped film. To gain more insight, the early fast energy transfer dynamic was also probed and the results of rise component shown in Figure 4(b) clearly indicate that **NOz-t-TPA** and **NOz-TPA** emission consists of a rise time of 893 ps and 692 ps, respectively. The time-resolved measurements for other doping concentration were also conducted with data shown in Figure S3 and Table 2. Two remarks can be promptly pointed out according to Figure 4(a) and Figure 4(b). Firstly, under the identical experimental condition, as shown in Figure 4(a), the delayed component of **NOz-TPA** doped film is nearly two folds shorter than that of **NOz-t-TPA** doped film. Secondly, the slightly faster rise time for the emission of **NOz-TPA** (cf. **NOz-t-TPA**) suggests faster energy transfer rate between exciplex host and **NOz-TPA**. Both observations significantly influence their performance on OLED. Detailed quantitative analyses are elaborated below.

Analysis in energy transfer dynamics

For clarity, we first probed the dynamics of the formation of exciplex between Tris-PCz and CN-T2T for host. The result shown in Figure S4(a) indicates that upon 357 nm excitation (repetition rate of 82kHz and pulse duration time of 180 fs) and monitoring at 500 nm exciplex emission the rise time is irresolvable (< 20 ps). Since the time constant for the formation of exciplex is much faster than all other kinetic parameters, the exciplex singlet CT state (S*(CT)) can be assumed to be populated instantaneously at t = 0 prior to any energy transfer processes. Standing on this basis, we tentatively propose an energy transfer mechanism depicted in Figure 5(b), which incorporates transfer of energy from TADF exciplex S*(CT) state and triplet T*(CT) state to the fluorescent dopant in the singlet (DS*) and triplet (DT*) manifolds. For the convenience of kinetic derivation, we simplify S*(CT) and T*(CT) to S* and T*, respectively, in the following text. This proposed energy transfer mechanism is commonly adopted the but never being rigorously validated in a quantitative manner, especially the competitive S* → DS* and T* → DT* processes, which are interplayed due to the thermally accessible process between and S* and T* reversibly because of their origin from TADF host. Mechanism depicted Figure 5(b) is utilized to fit the experimental data obtained in this study. Prior to the following fitting process, we have fully deconvoluted the measured population lifetime with instrumental response function (IRF), eliminating the broadening effect. For the detailed deconvolution process, please see **Simulative Approach** in **ESI**. We first attempted to fit the population evolution of pure TADF host (Tris-PCz:CN-T2T) with the following equations:

$$\frac{dS^*}{dt} = -\left(k_f + k_{isc}\right)\cdot S^*(t) + k_{risc}\cdot T^*(t)\ , \qquad (1)$$

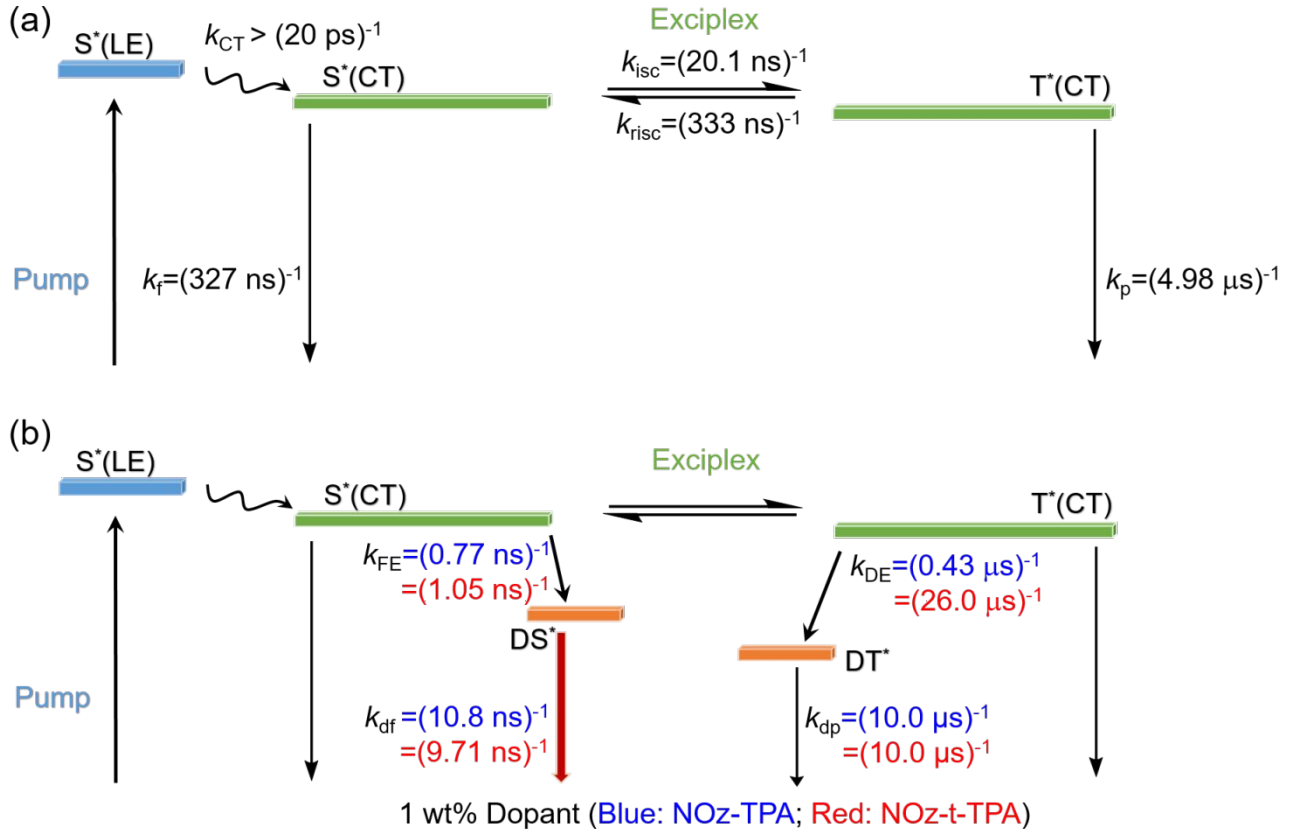

Figure 5. The proposed kinetic model for energy transfer process between exciplex host and fluorescent dopants in (a) Tris-PCz:CN-T2T and (b) Tris-PCz:CN-T2T:1 wt% dopant (Blue words for **NOz-TPA** and red words for **NOz-t-TPA**) solid thin film. Parameters k_{CT} is the rate of the formation of singlet CT state S*(CT) from localized excited state S*(LE); k_f and k_p are the population decay rate constants for the S*(CT) and triplet T*(CT) states of the exciplex (Tris-PCz:CN-T2T); k_{isc} and k_{risc} are intersystem crossing and reverse intersystem crossing rate constants, respectively. k_{FE} is FRET rate constant from exciplex S*(CT) to singlet state of dopant DS*, and k_{DE} is DET rate constant from exciplex T*(CT) to triplet states of dopant DT*. k_{df} and k_{dp} are the population decay rate constants of DS* and DT*, respectively.

$$\frac{dT^*}{dt} = -\left(k_p + k_{risc}\right)\cdot T^*(t) + k_{isc}\cdot S^*(t) \quad (2)$$

Here, k_f and k_p denote the observed decay rate of fluorescence and phosphorescence, respectively. k_{isc} and k_{risc} represent the intersystem crossing and reverse intersystem crossing rate constant, respectively, of exciplex. We initially guessed k_{isc}, k_{rsic}, k_f, and k_p to be (21.9 ns)$^{-1}$, (357 ns)$^{-1}$, (1 μs)$^{-1}$, and (10 μs)$^{-1}$, respectively, according to the previous work that assumed the pre-equilibrium between the exciplex CT S_1 and T_1 states.[6] These parameters were fitted iteratively with one parameter free to fit. As a result, we obtained the best fit shown in Figure S5(a) after several loops of adjustment for the parameters. k_{isc}, k_{risc}, k_p, and k_f were fitted to be (20.1 ns)$^{-1}$, (333 ns)$^{-1}$, (4.98 μs)$^{-1}$, and (327 ns)$^{-1}$, respectively. We then plugged in all parameter to eqs. (1-2) to calculate the prompt and delayed decay rates. The results of (17.9 ns)$^{-1}$ and (2.82 μs)$^{-1}$ for prompt and delayed fluorescence, respectively (Figure S5(b) and eq. (3) below) highly reproduce the experimental value of (20.8 ns)$^{-1}$ and (2.69 μs)$^{-1}$ (see Figure S4 (b)).

$$S^*(t) = 0.95\cdot e^{-t/17.9ns} + 0.05\cdot e^{-t/2.82\mu s} \quad (3)$$

For the convenience of discussion, all fitted parameters are shown in Figure 5(a). These deduced TADF kinetic parameters are then applied as the initial guessed values for the photoluminescence data of Tris-PCz:CN-T2T:1 wt% dopant

For the convenience of discussion, all fitted parameters are shown in Figure 5(a). These deduced TADF kinetic parameters are then applied as the initial guessed values for the photoluminescence data of Tris-PCz:CN-T2T:1 wt% dopant (**NOz-TPA**, **NOz-t-TPA**) solid thin film incorporating energy transfer model shown in Figure 5(b). Under the assumption of low doping concentration (1 wt% doped films), the direct excitation of dopants can be neglected (*vide supra*). Hence, the decay process of each excited species can be expressed as follows:

$$\frac{dS^*}{dt} = -(k_f + k_{isc} + k_{FE})\cdot S^*(t) + k_{risc}\cdot T^*(t), \quad (4)$$

$$\frac{dT^*}{dt} = -(k_p + k_{risc} + k_{DE})\cdot T^*(t) + k_{isc}\cdot S^*(t), \quad (5)$$

$$\frac{dDS^*}{dt} = -k_{df}\cdot DS^*(t) + k_{FE}\cdot S^*(t), \quad (6)$$

$$\frac{dDT^*}{dt} = -k_{dp}\cdot DT^*(t) + k_{DE}\cdot T^*(t). \quad (7)$$

The parameters k_{df} and k_{dp} denote the observed decay rate of dopant's fluorescence and phosphorescence, respectively; k_{FE} and k_{DE} represent the rate constant of FRET and DET, respectively. Due to the ππ* character and hence large ΔE_{ST} between DS* and DT* it is reasonable to assume the trivial efficiency of intersystem crossing and that the decay of DT* doesn't influence the population evolution of DS*. Therefore, k_{dt} can be fixed as a small constant, which is reasonable set to be e.g. (10 μs)$^{-1}$.

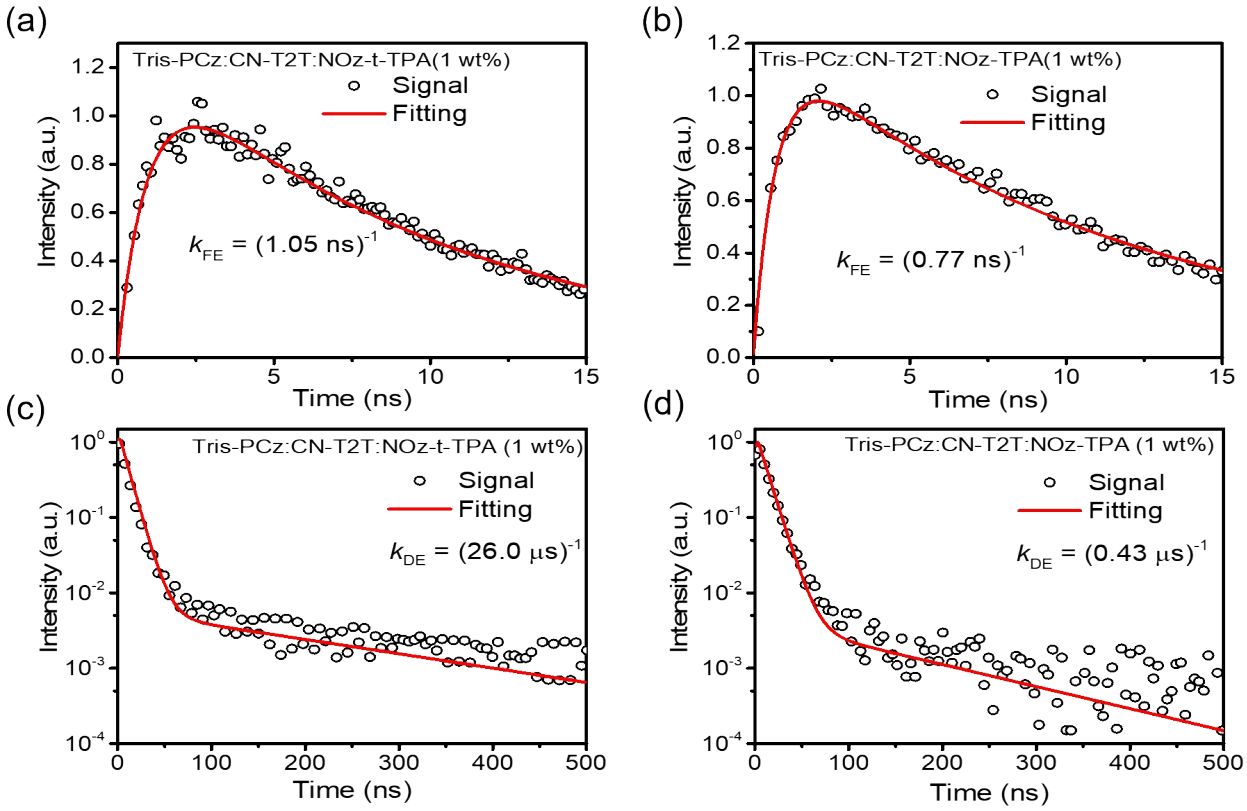

Figure 6. Model fitting of the population decay curve of (a, c) Tris-PCz:CN-T2T:1 wt% **NOz-t-TPA** and (b, d) Tris-PCz:CN-T2T:1 wt% **NOz-TPA** with rise component (a, b) and prompt-delayed component (c, d). Block circles are experimental data of two doped films acquired from TCSPC measurements under room temperature. Red lines are the fitting results for the population curves.

View Article Online
DOI: 10.1039/D0TC00986E

We initially guessed the TADF associated parameters k_{isc}, k_{risc}, k_f, and k_p to be (20.1 ns)$^{-1}$, (333 ns)$^{-1}$, (327 ns)$^{-1}$ and (4.98 μs)$^{-1}$, respectively, for the following fit. The dopant related parameters, k_{df} and k_{FE} of 1 wt% **NOz-t-TPA** were initially guessed to be (9.30 ns)$^{-1}$, and (893 ps)$^{-1}$, respectively, from its experimental prompt and rise lifetime; while for **NOz-TPA**, k_{df} and k_{FE} were initially guessed to be (10.8 ns)$^{-1}$ and (692 ps)$^{-1}$, respectively. As for k_{DE} of both emitters, we initially guessed them to be (1 μs)$^{-1}$ according to the literature.[47] The fitting process is separated into two parts, one for the rise component and the other for the prompt-delay component with the same parameters. Through the iterative fitting process, the best fit to the time-evolution of DS* for both **NOz-t-TPA** and **NOz-TPA** 1 wt% doped in the Tris-PCz:CN-T2T film is depicted in Figure 6(a,c) and Figure 6(b,d), respectively. Detailed fitting parameters for all rate constants are tabulated in Table S3. For the system with **NOz-t-TPA** as dopants, the associated rate constants for k_{FE} (FRET) and k_{DE} (DET) are thus determined to be (1.05 ns)$^{-1}$ and (26.0 μs)$^{-1}$, respectively, while they are (0.77 ns)$^{-1}$ and (0.43 μs)$^{-1}$, respectively, for **NOz-TPA** as the dopant. The resulted faster rate of k_{FE} (FRET) for **NOz-TPA** is consistent with the more spectral overlap between PL spectrum of exciplex and absorption spectrum of **NOz-TPA** (*vide supra*, see Figure 3(b)), supporting the validity of fitted k_{FE} parameters in terms of physical meaning. The analyses also indicate that the rate of Dexter type energy transfer k_{DE} (DET) for **NOz-t-TPA** is ~60 times slower than that for **NOz-TPA** doped in the Tris-PCz:CN-T2T film. This apparently results in the longer delayed component for **NOz-t-TPA** (cf. **NOz-TPA**, see Figure 4(a)). From the viewpoint of chemical structure, the hindrance in DET in **NOz-t-TPA** can be rationalized by the far separated distance between exciplexes and the core of dopant chromophore, i.e., **NOz-t-TPA**, because of four peripheral bulky *tert*-butyl groups anchored on the **TPA** moiety.

Taking all fitted parameters in Table S3, the analytical solutions of DS*(t) for both **NOz-TPA** and **NOz-t-TPA** are shown in eqs. (8-9) and their simulated curves are shown in Figure 7(a) where DS*(t=0) is normalized to be unity. Note that in this simulation a fourth exponential term originating from the decay of triplet state, DT* is omitted because of the forbidden transition. The simulated rise, prompt, and delayed lifetimes match the experimental fitted parameters shown in Table 2. However, these parameters are now endowed with physical meaning.

$$DS^*_{NOz-TPA}(t) = -1.00 \cdot e^{-t/717\,ps} + 1.00 \cdot e^{-t/10.79\,ns} + 3.29\times10^{-3} \cdot e^{-t/148\,ns} \quad (8)$$

$$DS^*_{NOz-t-TPA}(t) = 1.01 \cdot e^{-t/954\,ps} + 1.00 \cdot e^{-t/9.71\,ns} + 3.73\times10^{-3} \cdot e^{-t/228\,ns} \quad (9)$$

To compare the relatively steady state PL intensity between the doped films of **NOz-TPA** and **NOz-t-TPA**, we then integrate the simulated population curves from t = 0 to 1 s, followed by the multiplication with the corresponding k_r to simulate the fluorescence intensity. Here, we assume that the dopants in dilute concentration of 1 wt% should possess similar radiative

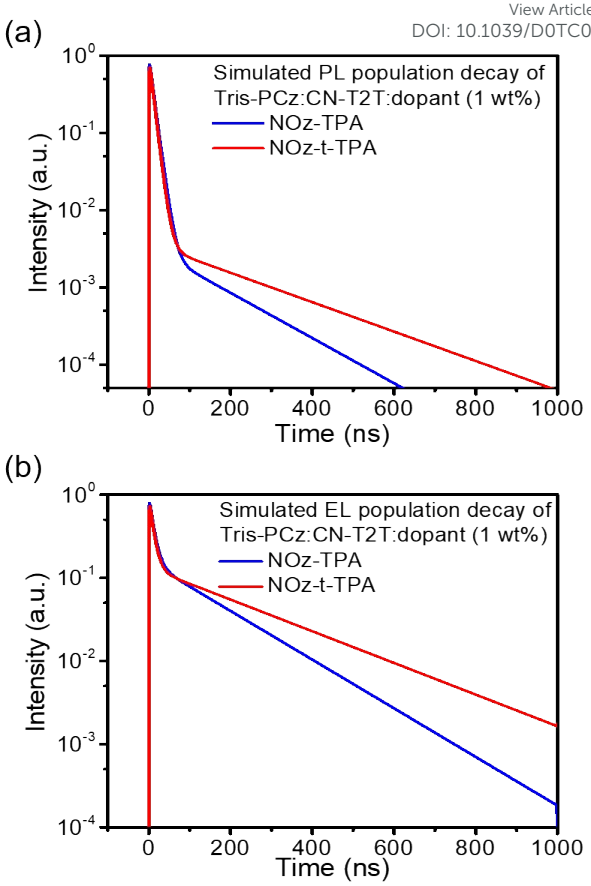

Figure 7. Simulated population decay of Tris-PCz:CN-T2T:dopant (1 wt%) under (a) PL and (b) EL.

behavior with that in toluene. Hence, we choose k_r measured in toluene as parameters, which are 8.81 × 10^7 and 7.62 × 10^7 s^{-1} for **NOz-TPA** and **NOz-t-TPA**, respectively. As a result, the PL intensity (I) ratio ($I_{NOz-t-TPA}$ / $I_{NOz-TPA}$) is deduced to be 0.79, consistent with the lower QY (28%) for **NOz-t-TPA** (cf. 42% for **NOz-TPA**).

Based on the simulation protocol we then made attempts to estimate the relative electroluminescence (EL) intensity. In this approach, the initial condition S*(0) and T*(0) is reset to be statistically 1 and 3, respectively, in equations (4) and (5) to generate the population curves for **NOz-t-TPA** and **NOz-TPA** 1 wt% doped in the Tris-PCz:CN-T2T film under electronic excitation. The results are shown in Figure 7(b). Upon integrating the area and multiplying the fluorescence radiative decay rate constant k_r for **NOz-t-TPA** (or **NOz-TPA**), the ratio of EL intensity for $I_{NOz-t-TPA}$ versus $I_{NOz-TPA}$ is estimated to be 1.04. Despite less intensity in PL, the simulation predicts better performance on EL of **NOz-t-TPA**. Although the real device performance also depends on other parameters such as device configuration and balance between electron and hole, etc., this methodology of using PL measurement serves as a paradigm to preliminarily estimate EL efficiency in OLEDs based on energy transfer between exciplex host and fluorescent guest. Its validity is further proved by the following practical EL measurement.

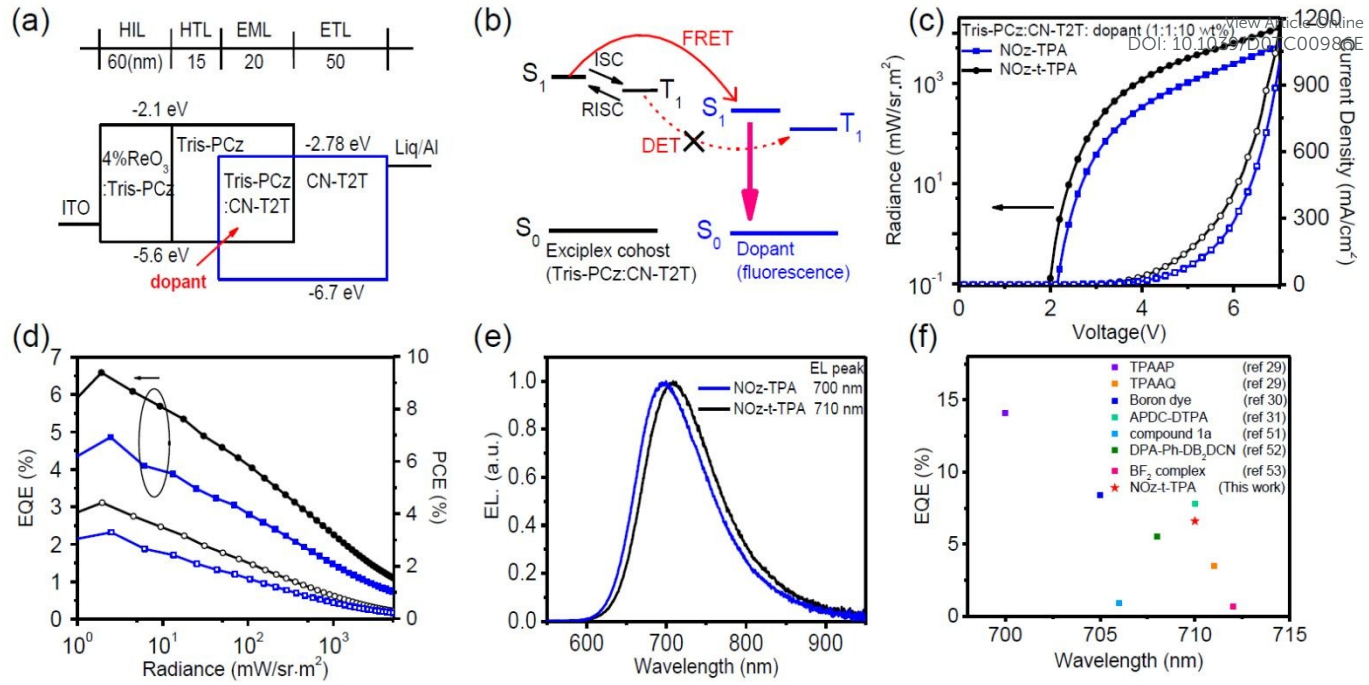

Figure 8. (a)Schematic energy level diagram of the device. (b) Schematic of the emission mechanism in exciplex cohost system doped with fluorophores. (c) Current density-voltage-radiance (J-V-R) characteristics. (d) External quantum efficiencies (EQE) and power conversion efficiencies (PCE) as a function of radiance. (e) EL spectra and (f) Comparison between NIR OLEDs in this work and other published metal-free NIR OLEDs.

Table 3. Electroluminescence Data of NIR OLED Devices.

dopant	X [%]	Von[a] [V]	[b]R/J at 7V [mW sr-1m-2/mA cm-2]	EQE/PCEmax [%/%]	λmax [nm]
NOz-TPA	1	2.2	14094/878	6.0/4.6	670
	5	2.2	5960/839	5.0/3.5	689
	10	2.2	5837/1012	4.3/3.0	700
NOz-t-TPA	1	2.0	60150/2160	7.4/5.3	683
	5	2.0	21310/1455	6.9/4.9	697
	10	2.0	12510/1160	6.6/4.4	710

[a]R is radiance and PCE is power conversion efficiency. [b]Turn-on voltage at which emission became detectable

Electroluminescence

Prior to the EL measurement, it is necessary to experimentally determine the energy level of HOMO and LUMO for title compounds in the solid thin film. To achieve this aim, photoelectron spectroscopy (PES) was conducted and the corresponding data are shown in Figure S6 and Table S3. Note that in the PES approach, the LUMO energy level was calculated from the corresponding orbital by adding the absorption energy gap in the solid neat film to the acquired HOMO level. For comparison, cyclic voltammetry measurement was also conducted in solution for acceptors (NOz) with corresponding data shown in Figure S7. Compared to other reported deep-red/NIR molecules with D-A-D systems, title compounds show relatively lower lying LUMO of -3.56 eV,[48-50] which suggest that NOz should be among the best acceptors for NIR D-A molecules.

EL properties of OLEDs were investigated by fabricating devicewith architectures of ITO/ 4wt% ReO_3: Tris-PCz (60 nm)/ Tris-PCz (15 nm)/ Tris-PCz:CN-T2T: 1, 5, 10 wt% dopant (20 nm)/CN-T2T (50 nm)/Liq (0.5 nm)/Al (100 nm) according to previous report.[6] Figure 8(a) shows the schematic energy level diagram of the device. According to the energy alignment the holes and electrons are able to be injected from Tris-PCz and CN-T2T to the emissive layer (EML) without any energy barrier, respectively. Figure 8(c)-(e) depicts the EL characteristics of the Tris-PCz:CN-T2T doped 10% **NOz-TPA** and **NOz-t-TPA** devices, and the key data are summarized in Table 3. We also show the EL characteristics with different doping concentration in Figure S8-S9. The device performance parameters are summarized in Table 3.

The 1 wt% **NOz-TPA** doping device exhibited maximum EQE and power conversion efficiency (PCE) of 6.0% and 4.6%, respectively, with an EL peak at 670 nm. However, at such low doping concentrations, the EL spectrum shows residual emission of exciplex. The 5 wt% **NOz-TPA** doping device displayed completely energy transfer. The EL displays a peak at

View Article Online DOI: 10.1039/D0TC00986E

689 nm and lower maximum EQE (5.0 %). When the doped concentration increases to 10%, the maximum EQE drops to4.3% as well as the EL peak redshift to 700 nm, respectively. As the doping concentration increases, the distance between guest molecules decreases, which increases the local polarization field and the increased local polarization field tends to cause the spectral redshift.[7] The lower efficiency might originate from the concentration quenching effects and the increase in DET from the triplet state (T_1) of exciplex to T_1 of dopant as Figure 8(b) shown. To eliminate the DET process from T_1 of the exciplex cohost to T_1 of the fluorescent emitters as well as to inhibit the concentration quenching process, a low doping concentration of the fluorescent emitter is thus required.

Notably, by adding *tert*-butyl groups on the para sites of phenyl rings in TPA, forming **NOz-t-TPA**, the NIR OLED devices have further high EQE and redshifted emission. When EML consists of low wt% such as 1% **NOz-t-TPA** to avoid the charge trapping process, the device displays maximum EQE of 7.4% and the EL spectrum shows clearly weak exciplex emission at 510 nm. Next, upon increasing the doping level of **NOz-t-TPA** to 5 wt%, the device displayed a radiance (R) of 21310 mW $sr^{-1}m^{-2}$ at 7.0 V (1455 mA cm^{-2}) with a peak at 697 nm, which achieved maximum EQE of 6.9% and PCE of 4.9%. Eventually, 10 wt% **NOz-t-TPA** as dopant, the device shows 71% of such emission falls in the NIR (> 700 nm) with an EL peaked at 710 nm. The remarkable point is that 10 wt% **NOz-t-TPA** device still maintains a maximum EQE of 6.6 %, which decreases a little compared to device with 5 wt% dopant (EQE of 6.9%). This suggests that the growth of DET accompanying the increase of doping level is not serious in **NOz-t-TPA** system (cf. **NOz-TPA**). The result is consistent with the early interpretation of PL results based on far separated distance between host material and guest molecules induced by the bulky *tert*-butyl substituent in **NOz-t-TPA** (*vide supra*), reaffirming the above kinetic analyses.

In regard to the current progress on the NIR OLEDs we then show a plot of the EL efficiency for the reported metal-free NIR OLEDs between 700 and 715nm in Figure 8(f).[29-31, 51-53] Clearly, this work presents an outstanding progress among the metal-free NIR OLED through the conventional organic fluorescent dyes pumped by exciplex host via energy transfer. And importantly, this study sheds light on the overall energy transfer mechanism that is of fundamental importance to the relevant research fields.

Conclusions

In summary, exploiting two newly designed D-A-D type fluorescence NIR emitters, **NOz-TPA** and **NOz-t-TPA**, we have gained fundamental insights into energy transfer pathways between exciplex host and fluorescent guest. Both chromophores are applied as the guest emitter to fabricate thin film with the exciplex host Tris-PCz:CN-T2T exiplex where the host acts as an energy donor. The PLQY of **NOz-TPA** and **NOz-t-TPA** NIR 680 nm and 709 nm emission are obtained to be 42 % and 28%, respectively, when optimized at 1 wt% blended in the Tris-PCz:CN-T2T film. Comprehensive time-resolved measurements suggest quiet different kinetic trace and hence energy transfer pathways between host and each fluorescence emitter. Detailed analyses conclude much different Dexter type of triplet-triplet energy transfer. Hindered by bulky *tert*-butyl substitution groups on the para sites of TPA, **NOz-t-TPA** doped film possesses ~60 times slower DET rate. Importantly, the analog analyses derived from the energy transfer mechanism (Figure 5) predict the relative PL and EL ratio for **NOz-t-TPA** versus **NOz-TPA** in the doped exciplex film. Despite the higher PL intensity in the **NOz-TPA** doped film, due to the original 75% population at the triplet state for which the energy dissipation is dominated by Dexter type energy transfer, **NOz-t-TPA** doped film predicts better OLED performance regarding e.g. EQE and PCE. This is further firmly proved by the real OLED operation (Figure 8 and Table 3). Correlated well with the analytical approach, the device of **NOz-t-TPA** displays a NIR emission peak at 710 nm with EQE up to 6.6%. This methodology incorporating comprehensive kinetic analyses proves to be powerful for exciplex host/fluorescent guest type of OLED, which may play a crucial role in guiding further NIR OLED development.

Conflicts of interest

There are no conflicts to declare.

Acknowledgements

This work was supported by the funding from Ministry of Science and Technology (MOST), featured areas research program within the framework of the Higher Education Sprout Project administrated by Ministry of Education (MOE) of Taiwan. We are grateful to the National Center for the High-performance Computing (NCHC) of Taiwan for the valuable computer time and facilities. We are thankful for the TGA data from Thermal Analysis System of Instrumentation Center, National Taiwan University. Z. Z. thanks the Program for Professor of Special Appointment (East-ern Scholar) at Shanghai Institutions of Higher Learning and the Start-up Grant of the East China University of Science and Technology (SP1901J010).

Notes and references

‡ CCDC number 1984380 contains the X-ray crystallographic coordinates for the compound **NOz-TPA** reported in this article. These data can be obtained free of charge from The Cambridge Crystallographic Data Centre via www.ccdc.cam.ac.

1 C. W. Tang and S. A. VanSlyke, *Appl. Phys. Lett.*, **1987**, *51*, 913-915.
2 M. A. Baldo, D. F.O 'Brien, Y. You, A. Shoustikov, S. Sibley, M. E. Thompson and S. R. Forrest, *Nature*, **1998**, *395*, 151.
3 H. Uoyama, K. Goushi, K. Shizu, H. Nomura and C. Adachi, *Nature*, **2012**, *492*, 234.
4 J. H. Burroughes, D. D. C. Bradley, A. R. Brown, R. N. Marks, K. Mackay, R. H. Friend, P. L. Burns and A. B. Holmes, *Nature*, **1990**, *347*, 539.
5 X.-K. Liu, Z. Chen, C.-J. Zheng, M.C hen, W. Liu, X.-H. Zhang and C.-S. Lee, *Adv. Mater.*, **2015**, *27*, 2025-2030.

6 W.-Y. Hung, P.-Y. Chiang, S.-W. Lin, W.-C. Tang, Y.-T. Chen, S.-H. Liu, P.-T. Chou, Y.-T. Hung and K.-T. Wong, *ACS Appl. Mater. Interfaces*, **2016**, *8*, 4811-4818.
7 B. Zhao, T. Zhang, B. Chu, W. Li, Z. Su, H. Wu, X. Yan, F. Jin, Y. Gao and C. Liu, *Sci. Rep.*, **2015**, *5*, 10697.
8 N. C. Giebink and S. R. Forrest, *Phys. Rev. B.*, **2008**, *77*, 235215.
9 D. L. Dexter, *J. Chem. Phys.*, **1953,** *21*, 836-850.
10 J.-C. G. Bünzli and S. V. Eliseeva, *J. Rare Earths*, **2010**, *28*, 824-842.
11 C.-L. Ho, H. Li and W.-Y. Wong, *J. Organomet. Chem.*, **2014**, *751*, 261-285.
12 G. Qian and Z. Y. Wang, *Chem. Asian. J.*, **2010**, *5*, 1006-1029.
13 E. L. Williams, J. Li and G. E. Jabbour, *Appl. Phys. Lett.*, **2006**, *89*, 083506.
14 M. Sauer, *Angew. Chem. Int. Ed.*, **2003**, *42*, 1790-1793.
15 G. S. He, G. C. Xu, P. N. Prasad, B. A. Reinhardt, J. C. Bhatt and A. G. Dillard, *Opt. Lett.*, **1995**, *20*, 435-437.
16 R. Yang, R. Tian, J. Yan, Y. Zhang, J. Yang, Q. Hou, W. Yang, C. Zhang and Y. Cao, *Macromolecules*, **2005**, *38*, 244-253.
17 S. Wang, X. Yan, Z. Cheng, H. Zhang, Y. Liu and Y. Wang, *Angew. Chem. Int. Ed.*, **2015**, *54*, 13068-13072.
18 C. Li, R. Duan, B. Liang, G. Han, S. Wang, K. Ye, Y. Liu, Y. Yi and Y. Wang, *Angew. Chem. Int. Ed.*, **2017**, *56*, 11525-11529.
19 L. H. Slooff, A. Polman, F. Cacialli, R. H. Friend, G. A. Hebbink, F. C. J. M. van Veggel and D. N. Reinhoudt, *Appl. Phys. Lett.*, **2001**, *78*, 2122-2124.
20 N. Tessler, V. Medvedev, M. Kazes, S. Kan and U. Banin, *Science*, **2002**, *295*, 1506.
21 R. J. Curry and W. P. Gillin, *Appl. Phys. Lett.*, **1999**, *75*, 1380-1382.
22 J. Kido and Y. Okamoto, *Chem. Rev.*, **2002**, *102*, 2357-2368.
23 M. Cocchi, D. Virgili, V. Fattori, J. A. G. Williams and J. Kalinowski, *Appl. Phys. Lett.*, **2007**, *90*, 023506.
24 K. Tuong Ly, R.-W. Chen-Cheng, H.-W. Lin, Y.-J. Shiau, S.-H. Liu, P.-T. Chou, C.-S. Tsao, Y.-C. Huang and Y. Chi, *Nat. Photonics*, **2016**, *11*, 63.
25 X. Ai, E. W. Evans, S. Dong, A. J. Gillett, H. Guo, Y. Chen, T. J. H. Hele, R. H. Friend and F. Li, *Nature*, **2018**, *563*, 536-540.
26 M.B ixon, J. Jortner, J. Cortes, H. Heitele and M. E. Michel-Beyerle, *J. Phys. Chem.*, **1994**, *98*, 7289-7299.
27 R.E nglman and J. Jortner, *Mol. Phys.*, **1970**, *18*, 145-164.
28 C. Borek, K. Hanson, P. I. Djurovich, M. E. Thompson, K. Aznavour, R. Bau, Y. Sun, S. R. Forrest, J. Brooks, L. Michalski and J. Brown, *Angew. Chem. Int. Ed.*, **2007**, *46*, 1109-1112.
29 J. Xue, Q. Liang, R. Wang, J. Hou, W. Li, Q. Peng, Z. Shuai and J. Qiao, *Adv. Mater.* **2019**, *31*, e1808242.
30 D. H. Kim, A. D'Aleo, X. K. Chen, A. D. S. Sandanayaka, D. D. Yao, L. Zhao, T. Komino, E. Zaborova, G. Canard, Y. Tsuchiya, E. Choi, J. W. Wu, F. Fages, J. L. Bredas, J. C. Ribierre and C. Adachi, *Nat. Photonics*, **2018**, *12*, 98.
31 Y. Hu, Y. Yuan, Y. L. Shi, D. Li, Z. Q. Jiang and L. S. Liao, *Adv. Funct. Mater.*, **2018**, *28*, 1802597.
32 H. Lu, Y. Zheng, X. Zhao, L. Wang, S. Ma, X. Han, B. Xu, W. Tian and H. Gao, *Angew. Chem. Int. Ed.*, **2016**, *55*, 155-159.
33 Y. Xia, P. Yang, Y. Sun, Y. Wu, B. Mayers, B. Gates, Y. Yin, F. Kim and H. Yan, *Adv. Mater.*, **2003**, *15*, 353-389.
34 Z. R. Grabowski, K. Rotkiewicz and W. Rettig, *Chem. Rev.*, **2003**, *103*, 3899-4032.
35 K. R. Justin Thomas, J. T. Lin, M. Velusamy, Y. T. Tao and C. H. Chuen, *Adv. Funct. Mater.*, **2004**, *14*, 83-90.
36 M. S. A. Abdel-Mottaleb, R. O. Loutfy and R. Lapouyade, *J. Photochem. Photobio. A*, **1989**, *48*, 87-93.
37 Z. Zhang, F. Lin, H.-C. Chen, H.-C. Wu, C.-L. Chung, C. Lu, S.-H. Liu, S.-H. Tung, W.-C. Chen, K.-T. Wong and P.-T. Chou, *Energy Environ. Sci.*, **2015**, *8*, 552-557.
38 H. Sirringhaus, P. J. Brown, R. H. Friend, M. M. Nielsen, K. Bechgaard, B. M. W. Langeveld-Voss, A. J. H. Spiering, R. A. J. Janssen, E. W. Meijer, P. Herwig and D. M. de Leeuw, *Nature*, **1999**, *401*, 685.
39 K. Kawashima, Y. Tamai, H. Ohkita, I. Osaka and K. Takimiya *Nat. Commun.*, **2015**, *6*, 10085.
40 K. Kawashima, I. Osaka and K. Takimiya, *Chem. Mater.*, **2015**, *27*, 6558-6570.
41 T. Ishi-i, R. Hashimoto and M. Ogawa, *Asian. J. Org. Chem.*, **2014**, *3*, 1074-1082.
42 T. Yanai, D. P. Tew and N. C. Handy, *Chem. Phys. Lett.*, **2004**, *393*, 51-57.
43 Will W. H. Lee, Z. Zhao, Y. Cai, Z. Xu, Y. Yu, Y. Xiong, R. T. K. Kwok, Y. Chen, N. L. C. Leung, D. Ma, J. W. Y. Lam, A. Qin and B. Z. Tang, *Chem. Sci.*, **2018**, *9*, 6118-6125.
44 P. Murto, A. Minotto, A. Zampetti, X. F. Xu, M. R. Andersson, F. Cacialli and E. G. Wang, *Adv. Opt. Mater.*, **2016**, *4*, 2068-2076.
45 T. X. Liu, L. P. Zhu, C. Zhong, G. H. Xie, S. L. Gong, J. F. Fang, D. G. Ma and C. L. Yang, *Adv. Funct. Mater.*, **2017**, *27*, 1606384.
46 M. Sarma and K.-T. Wong, *ACS Appl. Mater. Interfaces*, **2018**, *10*, 19279-19304.
47 T. Lazarides, D. Sykes, S. Faulkner, A. Barbieri and M. D. Ward *Chem: Eur. J.*, **2008,** *14*, 9389-9399.
48 W.-Y. Hung, L.-C. Chi, W.-J. Chen, Y.-M. Chen, S.-H. Chou and K.-T. Wong, *J. Mater. Chem.*, **2010**, *20*, 10113-10119.
49 H.-F. Chen, T.-C. Wang, S.-W. Lin, W.-Y. Hung, H.-C. Dai, H.-C. Chiu, K.-T. Wong, M.-H. Ho, T.-Y. Cho, C.-W. Chen and C.-C. Lee, *J. Mater. Chem.*, **2012**, *22*, 15620-15627.
50 D. Li, Y. Hu and L.-S. Liao, *J. Mater. Chem. C*, **2019**, *7*, 977-985.
51 X. B. Du, J. Qi, Z. Q. Zhang, D. G. Ma and Z. Y. Wang, *Chem. Mater.*, **2012**, *24*, 2178-2185.
52 S. P. Wang, Y. Miao, X. J. Yan, K. Q. Ye and Y. Wang, *J. Mater. Chem. C*, **2018**, *6*, 6698-6704.
53 A. D'Aleo, M. H. Sazzad, D. H. Kim, E. Y. Choi, J. W. Wu, G. Canard, F. Fages, J. C. Ribierre and C. Adachi, *Chem. Commun.*, **2017**, *53*, 7003-7006.